THE JOURNAL OF BIOLOGICAL CHEMISTRY Vol. 275, No. 10, Issue of March 10, pp. 7109–7116, 2000
Printed in U.S.A.

Binding of an Antibody Mimetic of the Human Low Density Lipoprotein Receptor to Apolipoprotein E Is Governed through Electrostatic Forces

STUDIES USING SITE-DIRECTED MUTAGENESIS AND MOLECULAR MODELING*

(Received for publication, September 1, 1999, and in revised form, December 14, 1999)

Robert Raffaï‡§¶, Karl H. Weisgraber§, Roger MacKenzie‖, Bernhard Rupp, Eric Rassart‡‡, Tomoko Hirama‖, Thomas L. Innerarity§, and Ross Milne‡§§**

*From the ‡Lipoprotein and Atherosclerosis Group, University of Ottawa Heart Institute, Ottawa Civic Hospital, Ottawa, Ontario K1Y TW7, Canada, the §Gladstone Institute of Cardiovascular Disease and the Cardiovascular Research Institute, University of California, San Francisco, California 94141-9100, the **Lawrence Livermore National Laboratory, Livermore, California 94550-9234, the ‖Institute for Biological Sciences, National Research Council of Canada, Ottawa, Ontario K1A 0R6, Canada, and the ‡‡Département des Sciences Biologiques, Université du Québec à Montréal, CP 8888, Montréal, Québec H3C 3P8, Canada*

Monoclonal antibody 2E8 is specific for an epitope that coincides with the binding site of the low density lipoprotein receptor (LDLR) on human apoE. Its reactivity with apoE variants resembles that of the LDLR: it binds well with apoE3 and poorly with apoE2. The heavy chain complementarity-determining region (CDRH) 2 of 2E8 shows homology to the ligand-binding domain of the LDLR. To define better the structural basis of the 2E8/apoE interaction and particularly the role of electrostatic interactions, we generated and characterized a panel of 2E8 variants. Replacement of acidic residues in the 2E8 CDRHs showed that Asp^{52}, Glu^{53}, and Asp^{56} are essential for high-affinity binding. Although Asp^{31} (CDRH1), Glu^{58} (CDRH2), and Asp^{97} (CDRH3) did not appear to be critical, the $Asp^{97} \rightarrow$ Ala variant acquired reactivity with apoE2. A $Thr^{57} \rightarrow$ Glu substitution increased affinity for both apoE3 and apoE2. The affinities of wild-type 2E8 and variants for apoE varied inversely with ionic strength, suggesting that electrostatic forces contribute to both antigen binding and isoform specificity. We propose a model of the 2E8·apoE immune complex that is based on the 2E8 and apoE crystal structures and that is consistent with the apoE-binding properties of wild-type 2E8 and its variants. Given the similarity between the LDLR and 2E8 in terms of specificity, the LDLR/ligand interaction may also have an important electrostatic component.

ApoE, a 34-kDa protein composed of 299 amino acids, is an important functional component of chylomicrons and very low, intermediate, and high density lipoproteins. As a ligand for the low density lipoprotein receptor (LDLR)[1] and for other members of the LDLR family, it plays an important role in the metabolism of plasma lipoproteins. ApoE exists as three common isoforms: apoE2, apoE3, and apoE4. The most common isoform, apoE3, has cysteine and arginine at positions 112 and 158, respectively, whereas apoE2 has cysteine and apoE4 has arginine at both positions. ApoE2 binds poorly to the LDLR, and homozygous inheritance of the apoE2 allele is strongly associated with type III dyslipoproteinemia (1).

Several lines of evidence suggest that positively charged amino acids at positions 136–150 of apoE interact directly with the LDLR (2). The LDLR-binding site is in the 22-kDa amino-terminal domain, and the strongest lipid-binding region is in the 10-kDa carboxyl-terminal domain. In a lipid-free form, the 22-kDa amino-terminal domain is folded into an elongated four-helix bundle; basic residues that have been implicated in LDLR binding are situated on helix 4, where they form a region with strong electropositive potential (3). Arg^{158} does not participate directly in apoE-mediated binding to the LDLR, but its replacement by a cysteine in apoE2 causes the rearrangement of intramolecular salt bridges within the LDLR-binding site, altering the alignment of the positively charged residues of apoE that interact with the LDLR (4).

The LDLR, an integral membrane protein composed of 831 amino acids, mediates the uptake of lipoproteins through its ability to bind to apoE and apoB. The amino terminus of the LDLR contains the ligand-binding domain that is composed of seven imperfect repeats of 40 amino acids. Each repeat includes six conserved cysteine residues and a cluster of acidic residues near its carboxyl terminus. Although the dual specificity of the LDLR appears to result from homology between the LDLR-binding sites of apoE and apoB (5), the individual cysteine-rich repeats may participate differentially in apoE- and apoB-mediated binding (6). Recently, the nuclear magnetic resonance structures of cysteine-rich repeats 1 and 2 (7) and the crystal structure of repeat 5 have been determined (8). Repeat 5 forms a folded calcium cage, and the side chains of many of the conserved aspartic and glutamic acid residues are involved

* This work was supported in part by Heart and Stroke Foundation of Ontario Operating Grant T3142, National Institutes of Health Program Project Grant HL 41633, and United States Department of Energy Grant W-7405-ENG-48 (to the Lawrence Livermore National Laboratory). The costs of publication of this article were defrayed in part by the payment of page charges. This article must therefore be hereby marked "*advertisement*" in accordance with 18 U.S.C. Section 1734 solely to indicate this fact.

¶ Recipient of studentships from the Heart and Stroke Foundation of Canada and from the Fond pour la Formation de Chercheur et l'Aide à la Recherche.

§§ To whom correspondence should be addressed: Lipoprotein and Atherosclerosis Group, University of Ottawa Heart Inst., 40 Ruskin St., Ottawa, Ontario K1Y 4W7, Canada. Tel.: 613-761-5258; Fax: 613-761-5281; E-mail: rmilne@ottawaheart.ca.

[1] The abbreviations used are: LDLR, low density lipoprotein receptor; mAb, monoclonal antibody; CDRH, heavy chain complementarity-determining region; CDRL, light chain complementarity-determining region; PCR, polymerase chain reaction; rFab, recombinant Fab; PAGE, polyacrylamide gel electrophoresis; ELISA, enzyme-linked immunosorbent assay; PBS, phosphate-buffered saline; WT, wild-type; SPR, surface plasmon resonance.

in coordinating the divalent ion. Previously, these acidic residues were thought to be available for ionic interactions with the basic residues in the receptor-binding sites of apoE and apoB; however, these new structural observations have necessitated a reassessment of the existing models for the binding of the LDLR to its ligands (9).

2E8 is a monoclonal antibody (mAb) that binds to apoE and prevents apoE-mediated binding of lipoproteins to the LDLR. The epitope recognized by 2E8 corresponds to the LDLR-binding site on human apoE (10). Like the LDLR, 2E8 binds well with apoE3 and poorly with apoE2. Antibodies recognize chemical structures by presenting physical surfaces complementary to those of the antigen (11). The antigen-binding site, or paratope of an antibody, is composed mainly of amino acids residing within the three heavy and light chain complementarity-determining regions (12), which exist as looped structures extending from the surface of the folded variable domains (13). van der Waals, hydrophobic, and electrostatic interactions provide the binding energy that is required to form the immune complex. Electrostatic forces participate in the initial attraction of grossly compatible structures of oppositely charged surfaces. The subsequent burial of hydrophobic residues within the interface contributes most of the binding energy (14, 15). In total, mAb 2E8 contains seven acidic residues within its CDRHs (10), six of which are exposed to solvent in the crystal structure of the Fab fragment (16). Because the 2E8 epitope possesses arginines and lysines, electrostatic interactions may be a major determinant of the affinity and specificity of the antibody for apoE.

In addition to the striking similarities in the binding specificities of 2E8 and the LDLR, CDRH2 of 2E8 also contains elements of sequence homology to the ligand-binding domain of the LDLR. We have proposed that 2E8 is an antibody mimetic of the LDLR (10) and could potentially serve as a surrogate for this receptor in studies designed to elucidate the structural basis for the interaction between apoE and the LDLR. Although detailed structural information on the intact ligand-binding domain of the LDLR is not yet available, the crystal structure of the 2E8 Fab fragment has recently been solved (16). To investigate further the interaction of 2E8 with apoE, which may provide new insights into the mechanisms responsible for the binding of apoE to the LDLR, we characterized the antigen-binding properties of a number of 2E8 variants that were generated by *in vitro* mutagenesis. We propose a model of the 2E8·apoE immune complex that is consistent with the tertiary structures of the 2E8 paratope and its epitope on apoE and with the apoE-binding characteristics of the 2E8 variants.

EXPERIMENTAL PROCEDURES

Site-directed Mutagenesis of the 2E8 Heavy Chain—Mutant forms of 2E8 with amino acid substitutions within CDRH1, CDRH2, and CDRH3 were produced by splice overlap extension polymerase chain reaction (PCR) (17) using appropriately designed oligonucleotide primers. Additional CDRH2 variants were isolated from a 2E8 CDRH2 random library generated by splice overlap extension PCR with spiked oligonucleotide primers containing alterations in all codons except for those encoding residues 52a and 55.[2] Briefly, splice overlap extension PCR was performed as follows. Two overlapping mutant products were created by performing PCR with forward and reverse mutant oligonucleotides in conjunction with a 3′-reverse primer containing the *Spe*I restriction site and a 5′-forward primer containing the *Xho*I site. The spliced overlap mutant PCR product was gel-purified, digested with the two endonucleases, and subcloned into the pComb3 soluble expression vector as described previously (18). In all cases, the amplification conditions consisted of 30 repeated cycles on a Stratagene Robocycler PCR apparatus. Each cycle corresponded to three 1-min incubations set at 95, 65, and 72 °C, followed by a 2-min incubation at 72 °C at the end of the cycling period. All variant forms of the heavy chain were verified by dideoxy chain termination sequencing before expression.

Recombinant Fab Production and Purification—The production and purification of the 2E8 recombinant Fab (rFab) fragment have been described (18). Each rFab preparation was subjected to SDS-PAGE, resolved by isoelectric focusing PAGE (Bio-Rad) in parallel with the pure hybridoma-generated Fab fragment, and stained with Coomassie Blue. Human apoE was produced and purified as described previously (19).

Enzyme-linked Immunosorbent Assay (ELISA) of 2E8 rFab Fragments—The binding of 2E8 variants to immobilized apoE was measured by an indirect ELISA as previously described (18).

Sandwich ApoE ELISA of mAbs 2E8 and 3H1—The previously described sandwich apoE radioimmunometric assay (10) was modified for an ELISA format. Briefly, polystyrene Immulon II plates (Dynatech Laboratories Inc.) were coated with 100 μl of pure anti-apoE mAb 6C5 at a concentration of 2 μg/ml in PBS (pH 7.4) overnight. After a 1-h incubation with 200 μl of blocking solution (PBS containing 1% bovine serum albumin), 100-μl aliquots of serially diluted (in blocking solution) pure recombinant full-length apoE isoforms (10 μg/ml starting concentration) were added, and the mixtures were incubated for 4 h at 4 °C. The wells were emptied and rinsed four times with PBS containing 0.025% Tween 20. The plates were then filled with serially diluted anti-apoE mAb 3H1 or 2E8, which had been coupled to horseradish peroxidase (Bethyl Laboratories, Inc.), and were left to incubate for 4 h at room temperature. The plates were then washed with PBS containing 0.025% Tween 20, and the bound mAbs were revealed as described above for the indirect ELISA.

Surface Plasmon Resonance—Primary amine groups of apoE3, apoE2, or bovine serum albumin were covalently coupled to CM5 sensor chips (BIAcore) as described (10). The remaining active sites were blocked with ethanolamine, and the chip surfaces were exposed to antibody diluted in HEPES-buffered saline containing 10 mM HEPES (pH 7.4), 150 mM NaCl, 3.4 mM EDTA, and 0.005% (v/v) surfactant P-20. Equilibrium affinity constants were calculated by Scatchard analysis from the sensorgram data with BIAevaluation software (BIAcore).

Cysteamine Treatment of ApoE—Pure apoE2 was treated with cysteamine as described previously (20). Briefly, 1 mg of protein was dissolved in 6 M urea containing cysteamine at a final concentration of 1 M. The protein was incubated overnight at 4 °C and extensively dialyzed against 20 mM NH_4HCO_3. Cysteamine modification was monitored by isoelectric focusing PAGE as described (20).

Molecular Modeling—All structural models were generated with the molecular viewing program Insight II (Molecular Simulations) using the atomic coordinates for apoE3 (Protein Data Bank accession number 1NFN), apoE2 (Protein Data Bank accession number 1LE2), and the 2E8 Fab fragment (Protein Data Bank accession number 12E8). Energy minimization and docking of the antibody and antigen were performed with the program Discover in Insight II. Intermolecular electrostatic bonds were scored positive if candidate atoms were ≤4 Å. Accompanying steric clashes were determined by setting a van der Waals overlap at 0.4 in the "Bump" function.

RESULTS

Mutagenesis, Expression, and Analysis of the 2E8 Heavy Chain Variants—The primary structures of the three 2E8 CDRHs and a list of the variants of the 2E8 heavy chains that were produced by site-directed and random saturation mutagenesis are presented in Fig. 1. Each rFab fragment was expressed in *Escherichia coli* and purified to homogeneity (18). All of the rFab preparations were >95% pure as assessed by SDS-12% PAGE. The fragments comigrated with Fab fragments generated by papain digestion of 2E8 IgG (data not shown). To confirm the phenotypic differences among the variants, we used isoelectric focusing PAGE to resolve all of the mutants in which a charged amino acid had been changed to alanine. As expected, 2E8(Thr^{57} → Glu) migrated to a more acidic position than the wild-type 2E8 rFab fragment (referred to throughout as WT 2E8), which migrated to a more acidic position than the alanine mutants, all of which comigrated (data not shown).

Relative Affinities of the 2E8 Variants for ApoE3 and ApoE2—The relative affinities and isoform specificities of the

[2] R. Raffaï, K. H. Weisgraber, R. MacKenzie, B. Rupp, E. Rassart, T. Hirama, T. L. Innerarity, and R. Milne, unpublished data.

A

CDRH1

31	32	33	34	35
Asp	Tyr	Tyr	Ile	His

CDRH2

50	51	52	52a		53	54	55	56	57	58	59	60	61	62	63
Trp	Ile	Asp	Pro		Glu	Ile	Gly	Asp	Thr	Glu	Tyr	Val	Pro	Lys	Phe

198	199	200	201	202	203	204	205	206	207	208	209	210
Gly	Pro	Asp	Cys	Lys	Asp	Lys	Ser	Asp	Glu	Glu	Asn	Cys

Repeat 5 (LDLr)

CDRH3

95	96	97	98	99	100	100a	100b	101	102	103
Gly	His	Asp	Tyr	Asp	Arg	Gly	Arg	Phe	Pro	Tyr

B

CDRH1

Asp31→Ala

CDRH2

Trp50→Leu
Asp52→Ala
→Asn
Glu53→Gly
Asp56→Ala
→Asn
Thr57→Glu
Glu58→Ala
→Gln
Asp52,Glu58→Ala52,Asp58
Glu53,Ile54→Ala53,Ser54

CDRH3

Asp97→Ala
Asp99→Ala

FIG. 1. **Primary structures of the 2E8 CDRHs, repeat 5 of the ligand-binding domain of the LDLR, and the 2E8 variants produced by *in vitro* mutagenesis.** *A*, shown are the primary structures of the 2E8 CDRHs and repeat 5 of the human LDLR. The amino acid sequences of the three 2E8 CDRHs are indicated according to the numbering system of Kabat *et al.* (12). The amino acid sequence of consensus sequence repeat 5 of the human LDLR is presented below that of CDRH2. *B*, a series of 2E8 heavy chain variants with amino acid substitutions in CDRHs was generated by *in vitro* mutagenesis. The 2E8 heavy chain variants were coexpressed with the 2E8 light chain in *E. coli*.

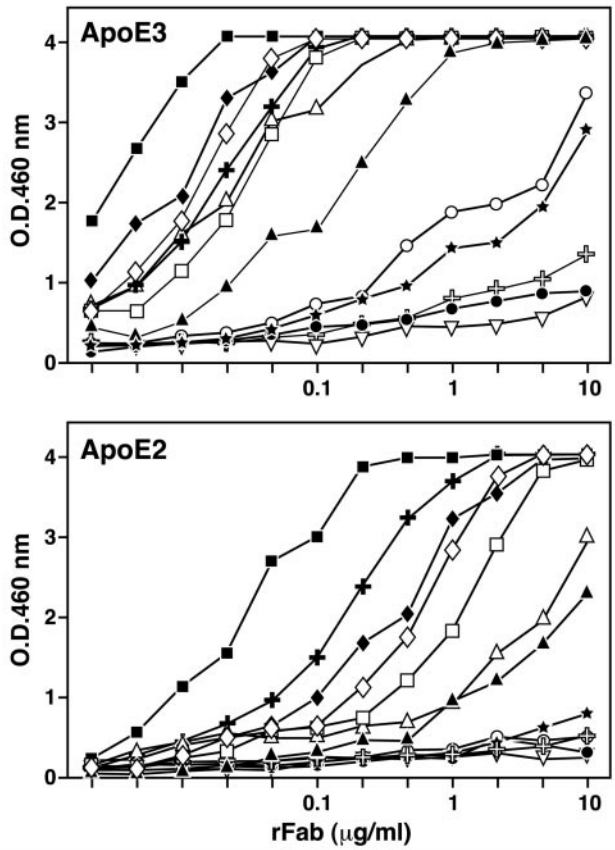

FIG. 2. **Relative immunoreactivities of WT 2E8 and 2E8 heavy chain variants with apoE3 (*upper panel*) and apoE2 (*lower panel*) under physiological salt conditions.** The relative immunoreactivities of WT 2E8 and 2E8 heavy chain variants were determined by an indirect solid-phase ELISA as described under "Experimental Procedures." In all cases, the highest antibody concentration was 10 μg/ml. ♦, WT 2E8; ■, Glu^{57}; △, Ala^{31}; ✚, Ala^{97}; ▽, Ala^{52}; ●, Asn^{52}; ○, Gly^{53}; ⋆, Ala^{56}; ✣, Asn^{56}; ◇, Ala^{58}; □, Gln^{58}; ▲, Leu^{50}.

TABLE I
Relative affinities of 2E8 rFab variants for human apoE3 and apoE2 determined by solid-phase immunoassay

Values represent the amounts of 2E8 rFab variants needed for 50% maximum binding to apoE isoforms at physiologic ionic strength.

2E8 rFab variant	ApoE3	ApoE2
	μg/ml	*μg/ml*
Wild-type	0.015	0.5
$Thr^{57} \rightarrow Glu$	0.003	0.03
$Asp^{31} \rightarrow Ala$	0.03	7
$Asp^{97} \rightarrow Ala$	0.02	0.15
$Asp^{52} \rightarrow Ala$	>10	>10
$Asp^{52} \rightarrow Asn$	>10	>10
$Glu^{53} \rightarrow Gly$	2.5	>10
$Asp^{56} \rightarrow Ala$	5	>10
$Asp^{56} \rightarrow Asn$	>10	>10
$Glu^{58} \rightarrow Ala$	0.02	0.6
$Glu^{58} \rightarrow Gln$	0.05	1.2
$Trp^{50} \rightarrow Leu$	0.15	6.5
$Asp^{52} \rightarrow Ala, Glu^{58} \rightarrow Asp$	>10	>10
$Glu^{53} \rightarrow Ala, Ile^{54} \rightarrow Ser$	>10	>10

rFab variants were assessed by determining their reactivity with immobilized apoE3 and apoE2 under conditions of physiological ionic strength in an indirect ELISA (Fig. 2). WT 2E8 was >35-fold more reactive with apoE3 than with apoE2 (Table I). The $Asp^{31} \rightarrow Ala$ substitution in CDRH1 decreased reactivity with both apoE3 (2-fold) and apoE2 (14-fold). In contrast, the reactivity of 2E8($Asp^{97} \rightarrow Ala$) with apoE3 decreased 1.3-fold, but increased 3-fold with apoE2 compared with WT 2E8. Thus, 2E8($Asp^{97} \rightarrow Ala$) continued to react preferentially with apoE3, but was less isoform-specific than WT 2E8. 2E8($Asp^{52} \rightarrow Ala$) did not react with apoE2 or apoE3, suggesting that Asp^{52} in CDRH2 is critical for binding to apoE. The $Glu^{53} \rightarrow Gly$ and $Asp^{56} \rightarrow Ala$ variants retained <1% of the apoE3-binding activity of WT 2E8. The defective apoE-binding activity of 2E8($Asp^{52} \rightarrow Ala$) and 2E8($Asp^{56} \rightarrow Ala$) could result from loss of the negative charges at positions 52 and 56 or from decreased topological complementarity with apoE. To distinguish between these possibilities, we tested variants in which Asp^{52} or Asp^{56} was replaced with asparagine. Because 2E8($Asp^{52} \rightarrow Asn$) and 2E8($Asp^{56} \rightarrow Asn$) displayed apoE-binding activities comparable to those of 2E8($Asp^{52} \rightarrow Ala$) and 2E8($Asp^{56} \rightarrow Ala$), respectively, formal negative charges appear to be required at positions 52 and 56. In the 2E8 crystal structure, Asp^{99} in CDRH3 is involved in an intramolecular hydrogen bond with CDRH3 Arg^{100b} and is not exposed to solvent. Although this hydrogen bond could be important in determining the conformation of the CDRH3 loop, the $Asp^{99} \rightarrow Ala$ variant has binding properties similar to those of WT 2E8 (data not shown). In contrast to what was observed with the other acidic residues in CDRH2, replacement of Glu^{58} with

TABLE II
Equilibrium affinity constants (K_d) for WT 2E8 and 2E8 variants with human apoE3 and apoE2 as determined by surface plasmon resonance
Measurements were performed at physiological salt concentration.

Variant	K_d	
	ApoE3	ApoE2
	μM	
Wild-type	3.8	ND[a]
$Thr^{57} \rightarrow Glu$	1.6	1.9
$Asp^{97} \rightarrow Ala$	5.0	6.4
$Asp^{31} \rightarrow Ala$	Weak binding	Weak binding
$Glu^{58} \rightarrow Ala$	17	ND
$Trp^{50} \rightarrow Leu$	59	ND

[a] No specific binding was detected.

alanine or glutamine resulted in variants with binding properties similar to those of WT 2E8. Neither the 2E8($Glu^{53} \rightarrow Ala$,$Ile^{54} \rightarrow Ser$) or 2E8($Asp^{52} \rightarrow Ala$,$Glu^{58} \rightarrow Asp$) double mutant bound to either isoform of apoE (Table I). 2E8($Thr^{57} \rightarrow Glu$) had 5-fold higher reactivity with apoE3 and 17-fold higher reactivity with apoE2 compared with WT 2E8. As with 2E8($Asp^{97} \rightarrow Ala$), the disproportional increase in the reactivity of 2E8($Thr^{57} \rightarrow Glu$) with apoE2 reduced apoE isoform specificity.

Equilibrium Affinity Constants for the 2E8 Variants with ApoE3 and ApoE2—To determine equilibrium binding constants for the most interesting of the 2E8 variants, we monitored the binding of the rFab fragments to apoE3 and apoE2 by surface plasmon resonance (SPR) (Table II). WT 2E8 had a K_d of 3.8 μM with apoE3, but did not bind apoE2. The affinity for apoE3 is lower than that of 2E8 IgG (K_d = 25 nM) (10), which most likely reflects the difference between monovalent and bivalent binding to the immobilized antigen. Consistent with the ELISA results, 2E8($Thr^{57} \rightarrow Glu$) had 2.5-fold higher affinity for apoE3 compared with WT 2E8. Surprisingly, 2E8($Thr^{57} \rightarrow Glu$) had the same binding affinity for apoE3 and apoE2 by SPR, but showed only a partial loss of apoE isoform specificity by ELISA (Fig. 2). Similarly, the loss of apoE isoform specificity of 2E8($Asp^{97} \rightarrow Ala$) was much more apparent with SPR than with ELISA. The decrease in the affinity of 2E8($Trp^{50} \rightarrow Leu$) was similar to that shown by ELISA (Fig. 2). These differences in the relative apoE isoform specificities of the 2E8 variants likely reflect inherent differences between the two techniques, particularly in the method of immobilizing apoE. In the solid-phase ELISA, apoE is noncovalently adsorbed to polystyrene microtiter wells, which can induce molecular rearrangements, unfolding, partial aggregation, and denaturation of the antigen (21). In SPR, apoE is covalently linked to a dextran matrix, which should allow the protein to be presented in a more native conformation. Another difference is that binding is measured over periods of seconds by SPR and hours by ELISA.

Effect of Salt on the Relative Affinities and Isoform Specificities of the 2E8 Variants—To investigate further the role of electrostatic interactions in the formation of the 2E8·apoE immune complex, we examined the effect of ionic strength on the binding of WT 2E8 to apoE3 in an indirect ELISA format (Fig. 3). Decreasing the concentration of NaCl below 150 mM increased binding, whereas higher concentrations decreased binding. Other monovalent salts (LiCl and KCl) gave results similar to those obtained with NaCl. However, the ability of WT 2E8 to bind to immobilized apoE3 was much more severely affected by the addition of the higher valency salts ($MgCl_2$, $CaCl_2$, and $LaCl_3$).

Next, we examined the effect of ionic strength on the isoform specificities of the 2E8 variants. All 2E8 variants showed their

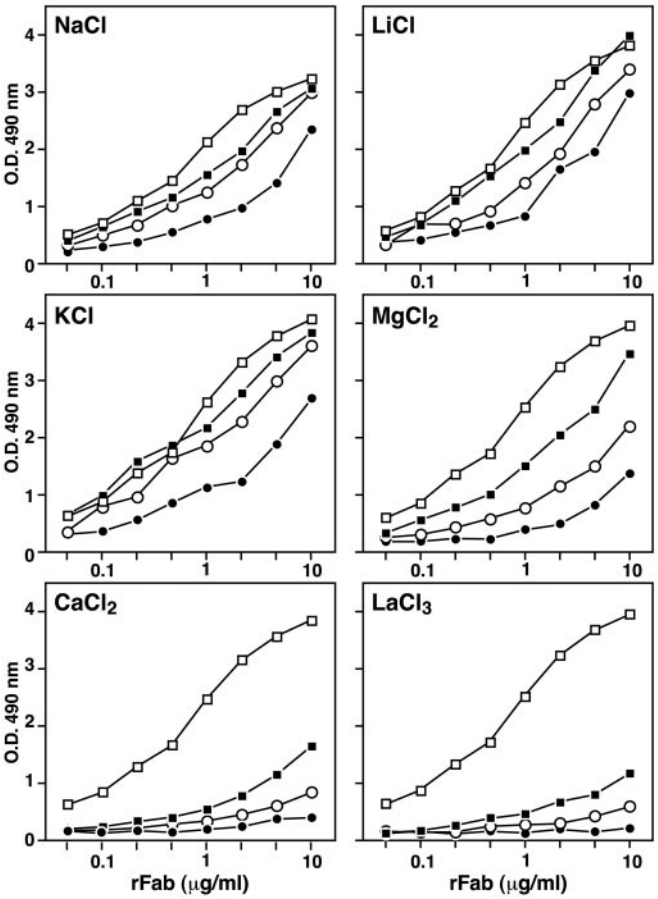

FIG. 3. **Effect of various salts and salt concentrations on the binding of WT 2E8 to apoE3.** Three monovalent salts (NaCl, KCl, and LiCl), two divalent salts ($MgCl_2$ and $CaCl_2$), and one trivalent salt ($LaCl_3$) were assessed. An indirect ELISA was used to determine the effect of salt valency and concentration on WT 2E8 binding to apoE3. In all cases, salt concentrations were 0–0.5 M in 20 mM Tris buffer (pH 7.2). □, 0 M salt; ■, 0.05 M salt; ○, 0.15 M salt; ●, 0.5 M salt.

greatest binding with both apoE2 and apoE3 in the absence of NaCl, with 2E8($Glu^{31} \rightarrow Ala$) showing the greatest proportional increase (data not shown). Whereas WT 2E8 maintained isoform specificity at this reduced ionic strength, 2E8($Glu^{31} \rightarrow Ala$), 2E8($Asp^{97} \rightarrow Ala$), and 2E8($Thr^{57} \rightarrow Glu$) reacted equally well with apoE3 and apoE2. Thus, the relative isoform specificities of WT 2E8 and the variants demonstrated by ELISA in the absence of NaCl resemble those demonstrated by SPR at physiological ionic strength. With NaCl concentrations above 150 mM, all of the variants maintained isoform specificity except for 2E8($Thr^{57} \rightarrow Glu$), which, by ELISA, showed preferential binding to apoE3 only at physiological ionic strength.

Immunoreactivity of WT 2E8 with Cysteamine-treated ApoE2 and ApoE2($Asp^{154} \rightarrow Ala$)—Treatment of apoE2 with cysteamine introduces a positive charge at residue 158 and restores the ability of apoE to mediate the binding of lipoproteins to the LDLR (22). Cysteamine-treated apoE2 was as reactive with mAb 2E8 as was apoE3 (Fig. 4). Although a positive charge appears to be required at apoE position 158 for binding to both the LDLR and 2E8, Arg^{158} does not participate directly in the interaction of apoE with the LDLR (4). In the crystal structure of apoE3, Arg^{158} forms salt bridges with Glu^{96} and Asp^{154} (Fig. 5). When Arg^{158} is replaced by Cys (as in apoE2), the side chains of Asp^{154} and Arg^{150} form a salt bridge, which causes both residues to be shifted from the positions that they occupy in apoE3. The shift of the Arg^{150} side chain out of the receptor-binding region is thought to be directly responsible for the

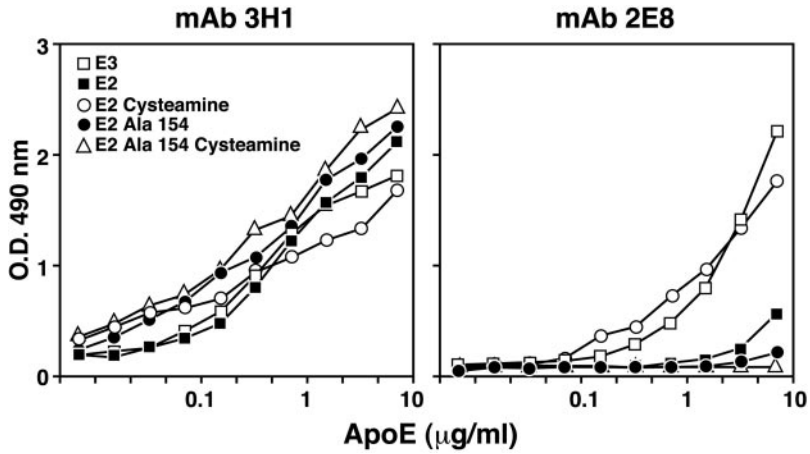

FIG. 4. **Effect of cysteamine treatment of apoE2 on mAb 2E8 binding monitored by direct solid-phase ELISA.** ApoE3, apoE2, apoE2(Asp^{154} → Ala), and cysteamine-modified apoE2 and apoE2(Asp^{154} → Ala) were coated onto polystyrene microtiter wells, and the individual amounts of immobilized apoE were measured with anti-apoE mAb 3H1 coupled to horseradish peroxidase (*left panel*). A second set of polystyrene microtiter wells, normalized for apoE content, was subjected to detection with horseradish peroxidase-linked mAb 2E8 (*right panel*).

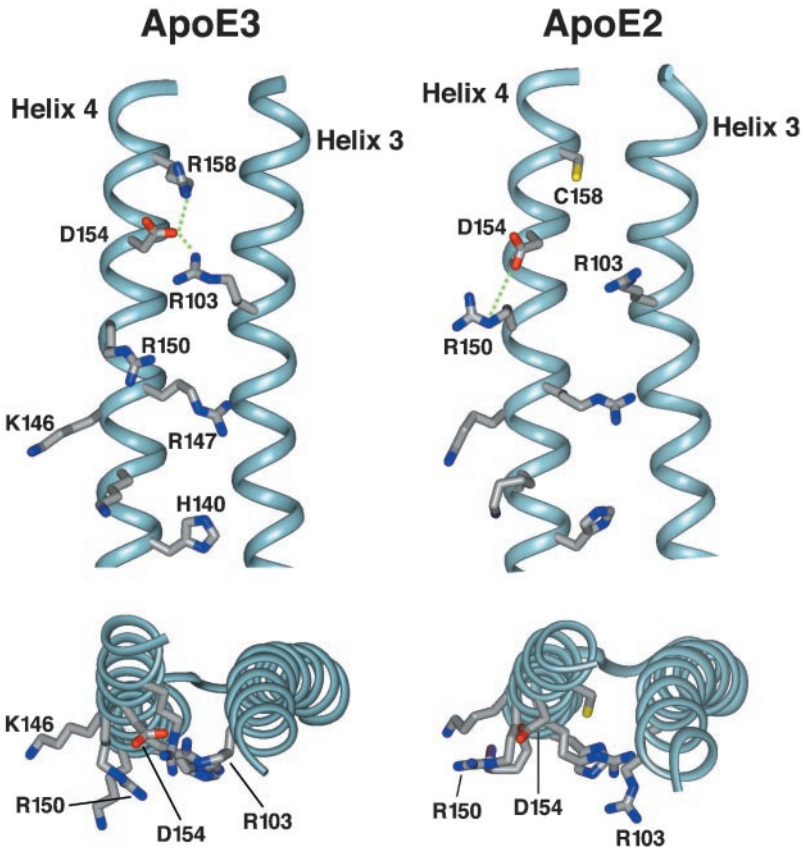

FIG. 5. **Structural variances in the orientation of the amino acid side chains of apoE3 and apoE2.** The structural variances in the side chain orientation of amino acids critical for 2E8 binding located on helices 3 and 4 of human apoE3 (*left*) and apoE2 (*right*) are shown. The superimposed ribbon drawings of the two isoforms are shown in two representations, rotated −90° about the *x* axis with respect to each other.

defective binding of apoE2 to the LDLR. Replacement of Asp^{154} by Ala in apoE2 disrupts the salt bridge between residues 150 and 154, allowing the side chain of Arg^{150} to occupy a position equivalent to that in apoE3. As a consequence, the apoE2(Asp^{154} → Ala) variant displays >80% of the LDLR-binding activity of apoE3 (4).

To determine if salt bridge arrangements are also critical for the isoform specificity of 2E8, we assessed the reactivity of 2E8 with apoE2(Asp^{154} → Ala) in a sandwich immunometric assay. In contrast to what was observed for the LDLR-binding activity, replacement of Asp^{154} with Ala in apoE2 did not increase 2E8 immunoreactivity (Fig. 4). Furthermore, there was no increase in 2E8 immunoreactivity when apoE2(Asp^{154} → Ala) was treated with cysteamine (Fig. 4). It is therefore probable that the side chain of Asp^{154} forms part of the 2E8 epitope. Although both the LDLR and 2E8 can differentiate apoE3 and apoE2 equally well, the structural basis for the isoform specificity may be different for the receptor and the antibody. In any case, electrostatic forces are likely to be involved.

Immunoreactivity of WT 2E8 with ApoE(Lys^{146} → Gln) and ApoE(Lys^{146} → Glu)—In our attempts to model the 2E8·apoE complex (see below), we observed that Lys^{146} in apoE appeared to make an important contribution to the binding to 2E8. To establish the participation of Lys^{146} in the formation of the 2E8·apoE complex, we tested the ability of WT 2E8 to bind to apoE(Lys^{146} → Gln) and apoE(Lys^{146} → Glu) by direct ELISA. The Glu^{146} variant was severely defective in 2E8 binding, whereas the Gln^{146} variant maintained high-affinity binding (Fig. 6). The same pattern of reactivity was observed with anti-apoE monoclonal antibody 1D7 (data not shown), which recognizes an epitope that overlaps the 2E8 epitope (10).

DISCUSSION

This study demonstrates that the acidic residues Asp^{52}, Glu^{53}, and Asp^{56} within CDRH2 of 2E8 are critical for high-affinity binding to apoE. The replacement of these residues

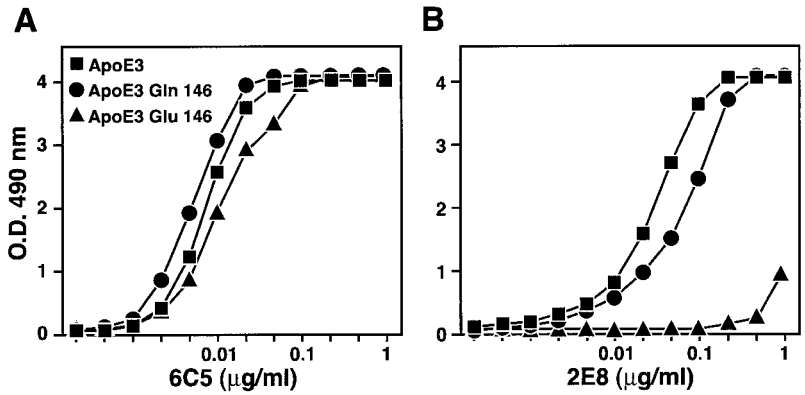

FIG. 6. **Relative immunoreactivities of mAb 2E8 with apoE3(Lys^{146} → Glu) and apoE3(Lys^{146} → Gln) as determined by a solid-phase ELISA.** Equivalent amounts of the apoE variants were coated onto polystyrene microtiter wells. The apoE-coated wells were normalized for apoE content using anti-apoE mAb 6C5, which was detected with horseradish peroxidase-linked rabbit anti-mouse IgG (*A*). The relative immunoreactivities of mAb 2E8 with the two apoE variants were determined by detecting bound mAb 2E8 with horseradish peroxidase-linked rabbit anti-mouse IgG (*B*).

resulted in a severe loss of apoE-binding activity, suggesting that formal negative charges are required at these positions for high-affinity binding. This study also demonstrates an inverse relationship between ionic strength and the binding of 2E8 to apoE, which suggests that electrostatic interactions are important in the formation of the 2E8·apoE immune complex.

Although Asp^{97} does not appear to be essential for the binding of 2E8 to apoE, 2E8(Asp^{97} → Ala) showed a loss of apoE isoform specificity. As measured by SPR under conditions of physiological ionic strength, the variant had similar affinity constants for apoE3 and apoE2. As measured by ELISA, however, the substitution exerted its full effect on isoform specificity only under conditions of reduced ionic strength. The loss of isoform specificity primarily reflected increased reactivity with apoE2 rather than decreased reactivity with apoE3. Asp^{97} therefore appears to dictate the apoE isoform specificity of WT 2E8. In the crystal structure of the 2E8 Fab fragment, the side chain of Asp^{97} lies on the periphery of the paratope (16). Replacement of Asp^{97} with alanine may create a cavity that can accommodate apoE side chains. Our model of the 2E8·apoE immune complex (described below) suggests that this apoE mass could originate from the side chain of apoE2 Arg^{103}. Introduction of a glutamic acid residue at position 57 of 2E8 CDRH2 results in a variant that has a small increase in affinity for apoE3 and a large increase in affinity for apoE2, resulting in similar equilibrium affinity constants for apoE3 and apoE2. We suggest that Glu^{57} forms a stabilizing ionic or hydrogen bond with Lys^{146} of apoE.

We previously reported that 2E8 and the LDLR have similar binding specificities for apoE isoforms (10). Substitution of neutral residues for basic residues within the apoE LDLR-binding site at positions 143, 145, 150, and 158 resulted in variants that bound defectively to both the LDLR (19) and 2E8 (10). Similarly, introduction of proline residues at positions 144 and 152 in apoE, which would be predicted to disrupt the secondary structure, prevented apoE from interacting with the LDLR and 2E8. We show here that a Lys^{146} → Glu (but not a Lys^{146} → Gln) substitution in apoE abolishes binding to 2E8. Finally, introduction of a positive charge at position 158 of apoE2 through cysteamine modification, known to restore LDLR-binding ability, restored the binding of apoE2 to the antibody. However, the LDLR and 2E8 react differently with apoE2(Asp^{154} → Ala). The replacement of Asp^{154} by Ala in apoE2 restored LDLR-binding activity to 80% of that of apoE3 (4). This variant does not react with 2E8, even after cysteamine treatment, suggesting that Asp^{154} is a critical residue in the 2E8 epitope, consistent with our model. The structural basis for the apoE isoform specificity of 2E8 could nevertheless be the same as that for the LDLR, although we cannot exclude the direct participation of Arg^{158} in the 2E8 epitope, which is not the case for the LDLR. Although residues 136–150 on helix 4 of

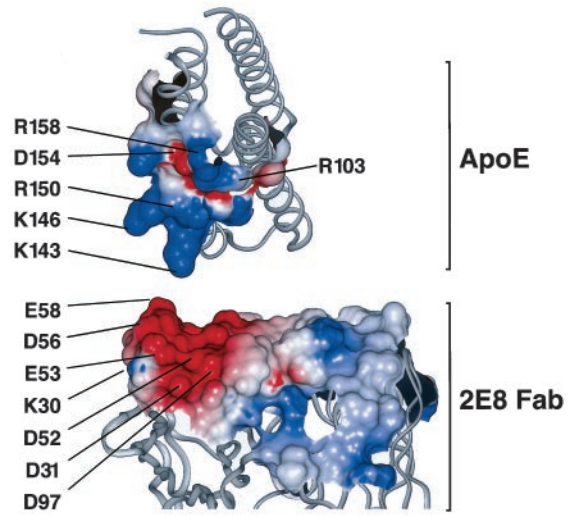

FIG. 7. **Electrostatic complementarity of the putative binding regions of apoE and mAb 2E8.** Solid surfaces were generated for the 2E8 CDRLs and CDRHs as was the LDLR-binding region of apoE (residues 142–158 and Arg^{103}) with Insight II. The surface-accessible charge was calculated with Delphi; *red* and *blue* indicate acidic and basic charges, respectively. The two structures are shown separated and slightly rotated about the *x* axis with respect to each other relative to the currently presented modeled complex form.

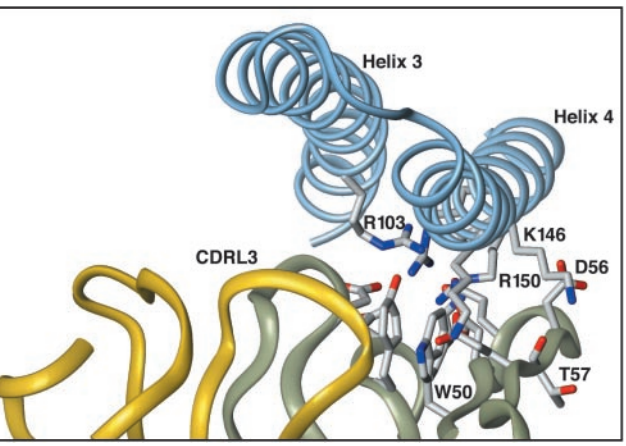

FIG. 8. **General shape complementary of the putative 2E8·apoE immune complex.** The general curvatures of apoE3 helices 3 and 4 are superimposed on the 2E8 paratope. Helix 4, which contains the basic amino acids required for high-affinity binding to both the LDLR and mAb 2E8, loops within the groove formed by the outer portion of CDRH2 and the crests of CDRL3 and CDRH3. The concave structure of helix 3 loops above the crest formed by CDRL3 and CDRH3. In this arrangement, regions of highest acidic potential in the 2E8 paratope overlap with the region of highest basic potential in the LDLR-binding site of apoE.

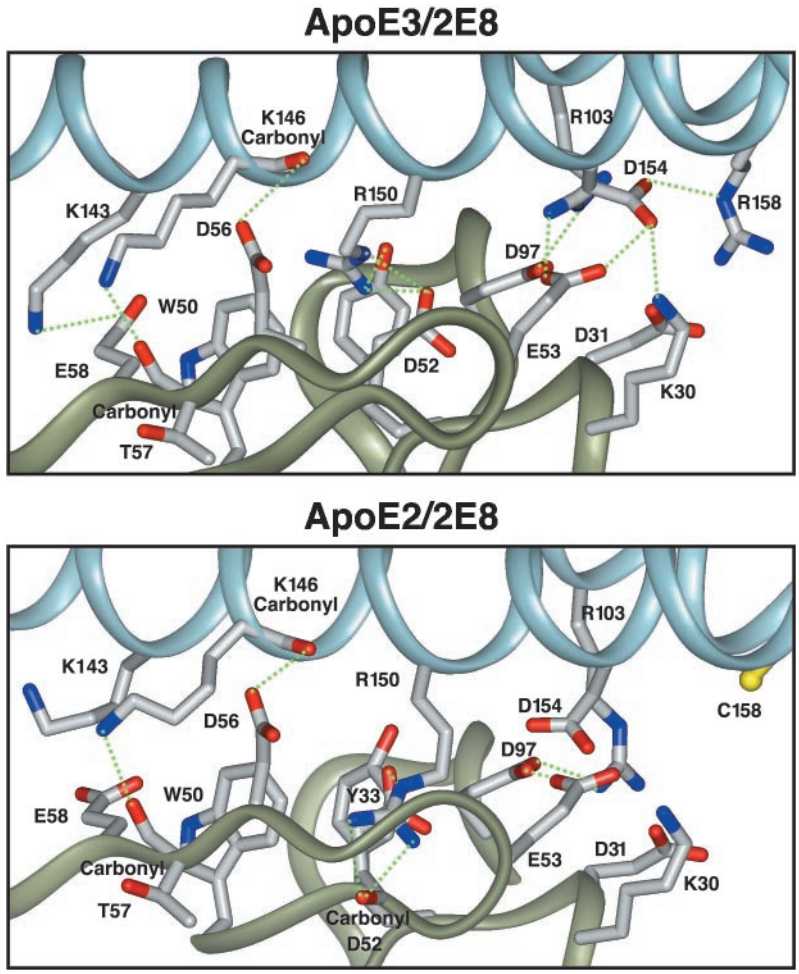

FIG. 9. **Predicted electrostatic interactions in the models of the 2E8·apoE3 (*upper panel*) and 2E8·apoE2 (*lower panel*) immune complexes.** Energy minimization of the putative 2E8·apoE immune complex shown in Fig. 8, first generated by the general shape and electrostatic complementarity of the two reactants, was submitted to energy minimization with the program Discover in Insight II. The computer-docked immune complexes between the apoE3 and apoE2 isoforms with mAb 2E8 are presented; *dotted lines* indicate potential electrostatic interactions. The distances between the candidate atoms are shown in Table III, which, in all cases, are ≤4 Å, and were simultaneously drawn with the "Measure Hbond" function in Insight II.

apoE clearly have a major role in the binding of apoE to the LDLR and 2E8, other residues may also contribute to binding. For example, our model of the 2E8·apoE3 immune complex suggests that Arg^{103} on helix 3 of apoE participates in the interaction.

The overall architecture of the 2E8 paratope consists of a relatively flat surface composed primarily of CDRHs coupled with an asymmetric distribution of surface-accessible electrostatic charge (Fig. 7). Within the portion of the paratope defined by CDRHs, a depression can be observed between the second half of CDRH2, which forms the outer rim of the paratope, and the crest of elongated CDRH3. The bottom of the depression is lined jointly by CDRH1 and the first half of the CDRH2 loop. As shown in Fig. 7, there is a striking complementarity in terms of electrostatic surfaces between the 2E8 epitope on apoE and the region of the 2E8 paratope that is contributed by CDRHs.

From the tertiary structures of 2E8 and apoE and the functional analysis described here, we developed a model of the 2E8·apoE3 immune complex, which was submitted to energy minimization analysis (Fig. 8). We propose that the 2E8 paratope is composed primarily of CDRHs and would recognize a discontinuous epitope on apoE that includes residues from the hydrophilic surfaces of helices 3 and 4 (Fig. 9). Most of the contact residues on apoE would be situated between residues 140 and 154 on helix 4. Both apoE helices, which are unusually elongated (3), adopt general curvatures that complement the positive and negative depressions formed by the 2E8 paratope (Fig. 8). Helix 4, which contains the basic residues required for high-affinity binding, loops within the depression of the 2E8 paratope. Furthermore, the convex curvature of helix 3 conforms well to the elevated portion of 2E8 formed conjointly by CDRH3 and CDRL3.

TABLE III

Computer-determined electrostatic interactions of the modeled 2E8 · apoE3 immune complex and accompanying intermolecular distances

The molecular model of the 2E8 · apoE immune complex was generated from general shape complementarity and from the current experimental mutational analysis. Electrostatic interactions were derived with the "Measure Hbond" function in the Insight II molecular viewing program. Electrostatic bonds were scored when a distance ≤4 Å separated two candidate atoms.

2E8 rFab (heavy chain)	ApoE3 intermolecular distance	ApoE2 intermolecular distance
	Å	
FRH1[a]		
Lys^{30} (NZ)	Asp^{154} (OD1), 2.8	
CDRH1		
Tyr^{33} (OH)	Arg^{150} (NH2), 2.8	
CDRH3		
Asp^{97} (OD1)	Arg^{103} (NE), 2.9	Arg^{103} (NH1), 2.7
Asp^{97} (OD2)		Arg^{103} (NH1), 2.7
CDRH2		
Asp^{52} (OD2)	Arg^{150} (NE), 2.6	Arg^{150} (NE), 2.8
Asp^{52} (OD2)	Arg^{150} (NH2), 2.8	
Asp^{52} (carbonyl)		Arg^{150} (NH1), 2.7
Asp^{52} (carbonyl)		Arg^{150} (NH2), 2.8
Glu^{53} (OE2)	Asp^{154} (OD1), 2.8	
Glu^{53} (OE1)	Arg^{103} (NH2), 2.8	
Asp^{56} (OD2)	Lys^{146} (carbonyl), 4.0	Lys^{146} (carbonyl), 3.9
Thr^{57} (carbonyl)	Lys^{146} (NZ), 3.0	Lys^{146} (NZ), 2.8
Glu^{58} (OE1)	Lys^{143} (NZ), 2.6	

[a] FRH1, heavy chain famework region 1.

Asp^{52} and Glu^{53} in 2E8 CDRH2 form an acidic pit within the depression of the 2E8 paratope (Figs. 7–9). In the 2E8·apoE

immune complex, apoE Arg^{150} would lie close to the 2E8 acidic pit. It would likely participate in favorable salt bridges or hydrogen bonds with the formally charged oxygen atoms of Asp^{52} and Glu^{53} or with the adjacent hydroxyl groups of residues such as Tyr^{33} and the backbone carbonyl of Lys^{30}. A salt bridge or hydrogen bond at the center of the protein-protein complex, an environment with a low dielectric constant, would be expected to have a high energetic value and, in addition, would permit the burial of some 80 $Å^2$ of apoE surface per arginine from solvent (23). This scenario would be consistent with the observed importance of Asp^{52} and Glu^{53} and apoE Arg^{150} in the antibody/antigen interaction. In the model, the side chains of Lys^{30} and Glu^{53} of the 2E8 heavy chain both contribute to stabilizing hydrogen bonds with apoE Asp^{154}. The energetic importance of Asp^{56} could be explained by the formation of a hydrogen bond between its side chain carboxylate and the main chain carbonyl group of apoE Lys^{146}.

According to our model, the formation of a salt bridge between Asp^{154} and Arg^{150} in apoE2 (Fig. 5) would effectively abolish three important interactions (Fig. 9). First, the burial of Arg^{150} within the 2E8 acidic pit would be hindered, with the concomitant loss of both a high-energy electrostatic bond in an area of low dielectric constant and favorable van der Waals interactions due to the large acyl side chain. Second, potential electrostatic bonds between Asp^{154} of apoE and Lys^{30} and Glu^{53} of the 2E8 heavy chain would be lost. The importance of Arg^{150} and Asp^{154} in the 2E8 epitope is apparent from the defective reactivity of apoE3($Arg^{150} \rightarrow$ Ala) and apoE2($Asp^{154} \rightarrow$ Ala). Introduction of a positive charge at residue 158 in apoE2 by cysteamine treatment would presumably reposition Arg^{150}, Asp^{154}, and Arg^{103}, allowing the 2E8 epitope to be restored. Although repositioned by energy minimization in our model, before computer docking, the side chain of Arg^{103} in apoE2 would severely clash with the WT 2E8 paratope, but not with that of the CDRH3($Asp^{97} \rightarrow$ Ala) variant, which would presumably accommodate the extra apoE mass due to the loss of the bulky carboxylate group (Fig. 9). As with CDRH2 Glu^{58}, the energy needed to physically distort the apoE and 2E8 side chains may outweigh the contributions of electrostatic bonds between these residues as predicted by the minimized complex.

Interestingly, through computer-assisted measurements and energy minimization of the 2E8·apoE3 immune complex, all of these experimentally derived intermolecular electrostatic interactions have been predicted to occur simultaneously, with minimal steric clashes and no changes to the main chain conformation of the two molecules (Table III). However, after energy minimization of the 2E8·apoE2 complex, the side chain of Arg^{150} was accommodated by distortion of the main chain conformation of CDRH2 Ile^{54}, which widened the CDRH2 loop by 1.5 Å, allowing for the formation of electrostatic bonds with the carboxylate group of CDRH2 Asp^{52}. The side chain of Arg^{103} was accommodated by the displacement of both this side chain and CDRH3 Asp^{97} in opposite directions, resulting in the concomitant formation of electrostatic interactions between the two residues. Evaluation of the intermolecular contact energies of the computer-docked complexes revealed large electrostatic contributions in both cases. Thus, a more severe intramolecular remodeling of both reactants, in addition to the loss of a few intermolecular electrostatic bonds, may well explain the lower binding affinities of apoE2 for the 2E8 antibody.

The finding that charged residues in both apoE and 2E8 are critical for binding suggests the involvement of electrostatic interactions and charge neutralization. Although it had been previously thought that a similar mechanism was responsible for the interaction of apoE with the LDLR, Fass *et al.* (8) have questioned this concept. In the crystal structure of cysteine-rich repeat 5, the side chains of many of the conserved acidic residues in the repeat that were thought to interact with basic residues in ligands of the LDLR are buried and participate in the coordination of a calcium ion. Fass *et al.* (8) also proposed that a hydrophobic concave surface of the cysteine-rich repeat provides a lipoprotein-binding surface. Alternatively, it has been suggested that other acidic residues within the cysteine-rich repeats, which are not implicated in the coordination of calcium, could be implicated in the interaction with ligands or that the conformation of individual repeats could be altered in the context of other repeats (9). Another possibility is that, under specific conditions (*e.g.* in the presence of ligand or lipoprotein surface lipid), the individual repeats could be amenable to conformational changes that could lead to the loss of tertiary structure among multiple repeats, revealing cryptic acidic residues. It may also be possible that the remaining exposed acidic side chains in conjunction with main chain carbonyl oxygens create a suitable electrostatic surface for apoE recognition. Although the exact mode of interaction of the LDLR and 2E8 with apoE need not be identical, the two molecules do recognize overlapping sites on apoE and show a remarkable similarity in their respective fine specificities. Given the importance of charge neutralization in the binding of apoE to 2E8, it would be surprising if this were not also the case for the interaction of apoE with the LDLR.

Acknowledgments—The pComb3 expression vector was kindly provided by Dr. Richard Lerner. We thank Dr. Paul C. R. Hopkins for critical input and Dr. Clare Peters-Libeu for help in computer modeling. We also thank Denise Murray for help with manuscript preparation, Gary Howard and Stephen Ordway for editorial assistance, and Neile Shea and John Carrol for help with the preparation of figures.

REFERENCES

1. Mahley, R. W., and Rall, S. C., Jr. (1995) in *The Metabolic and Molecular Bases of Inherited Disease* (Scriver, C. R., Beaudet, A. L., Sly, W. S., and Valle, D., eds.) 7th Ed., pp. 1953–1980, McGraw-Hill Book Co., New York
2. Weisgraber, K. H. (1994) *Adv. Protein Chem.* **45,** 249–302
3. Wilson, C., Wardell, M. R., Weisgraber, K. H., Mahley, R. W., and Agard, D. A. (1991) *Science* **252,** 1817–1822
4. Dong, L.-M., Parkin, S., Trakhanov, S. D., Rupp, B., Simmons, T., Arnold, K. S., Newhouse, Y. M., Innerarity, T. L., and Weisgraber, K. H. (1996) *Nat. Struct. Biol.* **3,** 718–722
5. Borén, J., Lee, I., Zhu, W., Arnold, K., Taylor, S., and Innerarity, T. L. (1998) *J. Clin. Invest.* **101,** 1084–1093
6. Russell, D. W., Brown, M. S., and Goldstein, J. L. (1989) *J. Biol. Chem.* **264,** 21682–21688
7. Bieri, S., Atkins, A. R., Lee, H. T., Winzor, D. J., Smith, R., and Kroon, P. A. (1998) *Biochemistry* **37,** 10994–11002
8. Fass, D., Blacklow, S., Kim, P. S., and Berger, J. M. (1997) *Nature* **388,** 691–693
9. Brown, M. S., Herz, J., and Goldstein, J. L. (1997) *Nature* **388,** 629–630
10. Raffaï, R., Maurice, R., Weisgraber, K., Innerarity, T., Wang, X., MacKenzie, R., Hirama, T., Watson, D., Rassart, E., and Milne, R. (1995) *J. Lipid Res.* **36,** 1905–1918
11. Davies, D. R., and Cohen, G. H. (1996) *Proc. Natl. Acad. Sci. U. S. A.* **93,** 7–12
12. Kabat, E. A., Wu, T. T., Perry, H. M., Gottesman, K. S., and Foeller, C. (1991) *Sequences of Proteins of Immunological Interest*, 5th Ed., National Institutes of Health, Bethesda, MD
13. Padlan, E. A. (1994) *Mol. Immunol.* **31,** 169–217
14. Novotny, J., and Sharp, K. (1992) *Prog. Biophys. Mol. Biol.* **58,** 203–224
15. Schreiber, G., and Fersht, A. R. (1996) *Nat. Struct. Biol.* **3,** 427–431
16. Trakhanov, S., Parkin, S., Raffaï, R., Milne, R., Newhouse, Y. M., Weisgraber, K. H., and Rupp, B. (1999) *Acta Crystallogr. Sect. D* **55,** 122–128
17. Higushi, R., Krummel, B., and Saiki, R. K. (1988) *Nucleic Acids Res.* **16,** 7351–7367
18. Raffaï, R., Vukmirica, J., Weisgraber, K. H., Rassart, E., Innerarity, T. I., and Milne, R. (1999) *Protein Expression Purif.* **16,** 84–90
19. Lalazar, A., Weisgraber, K. H., Rall, S. C., Jr., Giladi, H., Innerarity, T. L., Levanon, A. Z., Boyles, J. K., Amit, B., Gorecki, M., Mahley, R. W., and Vogel, T. (1988) *J. Biol. Chem.* **263,** 3542–3545
20. Weisgraber, K. H., Rall, S. C., Jr., and Mahley, R. W. (1981) *J. Biol. Chem.* **256,** 9077–9083
21. Djavadi-Ohaniance, L., and Friguet, B. (1991) in *Immunochemistry of Solid-Phase Immunoassay* (Butler, J. E., ed) pp. 201–205, CRC Press, Inc., Boca Raton, FL
22. Innerarity, T. L., Weisgraber, K. H., Arnold, K. S., Rall, S. C., Jr., and Mahley, R. W. (1984) *J. Biol. Chem.* **259,** 7261–7267
23. Clackson, T., Ultsch, M. H., Wells, J. A., and de Vos, A. M. (1998) *J. Mol. Biol.* **277,** 1111–1128